

Impurity-Ion pair induced high-temperature ferromagnetism in Co-doped ZnO

C.D. Pemmaraju^a, R. Hanafin^a, T. Archer^a, H.B. Braun^b and S. Sanvito^a

^a *School of Physics and CRANN, Trinity College, Dublin 2, Ireland and*

^b *School of Physics, University College Dublin, Dublin 4, Ireland*

(Dated: February 3, 2008)

Magnetic 3d-ions doped into wide-gap oxides show signatures of room temperature ferromagnetism, although their concentration is two orders of magnitude smaller than that in conventional magnets. The prototype of these exceptional materials is Co-doped ZnO, for which an explanation of the room temperature ferromagnetism is still elusive. Here we demonstrate that magnetism originates from Co^{2+} oxygen-vacancy pairs with a partially filled level close to the ZnO conduction band minimum. The magnetic interaction between these pairs is sufficiently long-ranged to cause percolation at moderate concentrations. However, magnetically correlated clusters large enough to show hysteresis at room temperature already form below the percolation threshold and explain the current experimental findings. Our work demonstrates that the magnetism in ZnO:Co is entirely governed by intrinsic defects and a phase diagram is presented. This suggests a recipe for tailoring the magnetic properties of spintronics materials by controlling their intrinsic defects.

ZnO is a piezoelectric conductive oxide, in which free-carriers coexist with optical transparency^{1,2}. If made magnetic, ZnO will become the ultimate multifunctional material, with semiconducting, magnetic, optical and mechanical properties. This will have a far reaching impact on the emerging field of spintronics³ with applications in optoelectronics⁴ and quantum computing⁵. Moreover it will allow us to go beyond the (Ga,Mn)As paradigm⁶, whose practical use is severely hampered by the low ferromagnetic critical temperature. This is why ZnO:Co is perhaps the most studied among all the diluted magnetic oxides. Room-temperature ferromagnetism (RTF), first demonstrated by Ueda et al.⁷, is now confirmed by a number of groups^{8,9,10} (see Table I of the supplementary material). The experimental situation is however still confused and here we list the main findings.

i) Spectroscopy confirms that Co^{2+} substituting Zn is the center responsible for all the different magnetic phases found experimentally, including RTF^{11,12,13}, paramagnetism^{12,14} and spin-glasses¹⁵. RTF is usually assigned from magnetometry^{7,8,9,10}.

ii) The saturation magnetization M_s and the remanence are always small and secondary phases are often difficult to rule out. However, except for metallic Co, most of them are either non-magnetic or antiferromagnetic with low Néel temperatures (CoO , Co_2O_3 , Co_3O_4 , ZnCo_2O_4). The coercive field is typically small (~ 100 Oe) and only weakly temperature dependent.

iii) M_s is usually smaller than what is expected for Co^{2+} with values as low as $0.01 \mu_B/\text{Co}^{12}$, suggesting antiferromagnetic interaction among Co^{2+} and frustration^{13,14,16}.

iv) Growth conditions and annealing are crucial for the magnetic state. Chemical methods^{14,16} and molecular beam epitaxy¹⁷ generally lead to paramagnetism, while pulsed laser deposition produces RTF films^{7,8,9,10}. Typically oxygen deficient growth¹⁰ at tuned substrate temperatures^{18,19,20} promotes RTF. Similarly, annealing in vacuum enhances the magnetic moment and produces ferromagnetism^{12,20,21,22}, while annealing in oxygen has

the opposite effect^{22,23}.

v) The role played by free carriers in establishing magnetism is unclear. Sequential annealing in reducing and oxidizing atmosphere reveals little correlation between the electrical conductivity and the magnetic state²⁴. Similar conclusions are reached for Al- and H-doping²⁵.

vi) ZnO is often reported to be oxygen deficient. This has been attributed to either oxygen vacancies (V_O)^{26,27} or multi-center H^{28} , with Zn interstitials (Zn_i) now ruled out by both experimental²⁶ and theoretical^{27,28} evidence. Thus the promotion of RTF due to Zn vapour exposure²⁹ cannot be attributed to an increase of the Zn_i concentration.

vii) Electron paramagnetic resonance³⁰ suggests the presence of two magnetic centers. These are both related to Co^{2+} , although they exhibit fine differences in the signal. Interestingly, for a nominal Co concentration about 5% the two centers appear with similar abundance.

Existing mechanisms for ferromagnetism in the diluted limit cannot explain this complex collection of phenomena. The p - d Zener model³¹ lacks of its foundations when applied to $\text{Zn}_{1-x}\text{Co}_x\text{O}$ since there is little correlation between carriers and magnetism^{24,25}. When present, carriers are electrons and not holes with small exchange coupling to the local spins and therefore the typical critical temperatures (T_C) are tiny at realistic carrier densities. Similarly super-exchange must be ruled out³². This is short ranged and RTF can be obtained only for x above the nearest neighbour (NN) percolation threshold. For the wurtzite lattice this is 20 %, much greater than the typical experimental concentrations.

Finally a modification of the Zener scheme, called the “donor impurity band exchange” (DIBE), assumes that the magnetic interaction is mediated by large hydrogenic orbitals associated to intrinsic defects and predicts ferromagnetism below the donor percolation threshold, i.e. in absence of free carriers³³. Although the mean field T_C obtained with realistic parameters for $\text{Zn}_{1-x}\text{Co}_x\text{O}$ is extremely small (~ 10 K)³³, the model is frequently used to explain the experimental results. We have investigated

such a model with Monte Carlo calculations (see supplementary materials) and demonstrated that for Co and donor concentrations respectively of 10 % and 1 %, the T_C is only a few degrees K. RTF is obtained only with unrealistically high values of the exchange coupling, and therefore the DIBE scheme must also be ruled out.

In the absence of any simple-scheme for ferromagnetism we turn to atomistic density functional theory (DFT). For this problem the standard approximations to the exchange and correlation potential (LDA and GGA) are not appropriate since they over-delocalize and under-bind the Co- d shell resulting in their incorrect positioning with respect to the Fermi level, E_F . These failures are only minor in the case of GaAs:Mn³⁴, but they become a serious drawback for the oxides where the Co d density of states (DOS) has important contributions in the ZnO band-gap. We therefore use an approximated version of the self-interaction correction (ASIC) scheme³⁵, which is free from these problems and produces exchange parameters for transition metal monoxides superior to those obtained with LDA/GGA³⁶.

In Fig. 1 we present the DOS of a Co impurity (at the Zn site) in a 128 atom ZnO supercell ($x=0.0156$) calculated with both LDA and ASIC. Although they both predict a 2+ valence, the position of the Co d levels is remarkably different in the two cases. LDA places the

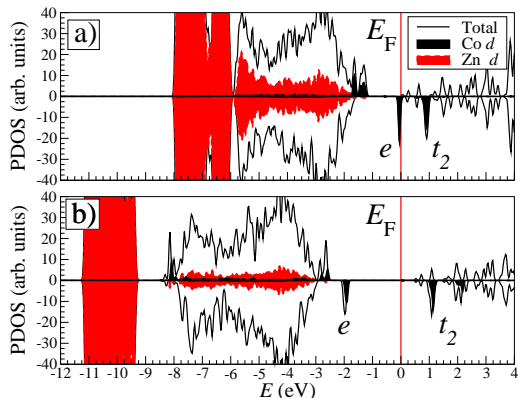


FIG. 1: Density of states of $\text{Zn}_{1-x}\text{Co}_x\text{O}$ as calculated from density functional theory. The simulation cell is a 128 ZnO supercell in which one Zn atom is replaced by Co ($x=0.0156$). Panels (a) and (b) show LDA and ASIC results respectively.

occupied minority e states just below E_F at the edge of the ZnO conduction band minimum (CBM). ASIC shifts these by about 2 eV down to the valence band top (VBT) in agreement with recent calculations³⁷. In addition the ZnO band-gap opens and the Zn d DOS is also down-shifted. This gives us a picture where there is no Co- d contribution to the DOS around E_F , with the first unoccupied minority states (t_2) placed at about 1 eV above the CBM. Such a DOS is in excellent agreement with ultraviolet photoemission (UPS), which places the Co d DOS at a binding energy of about 3 eV with a satellite peak at 7 eV and a rather diffuse tail¹³. This electronic

structure is incompatible with a carrier mediated picture of ferromagnetism. In fact, E_F should be moved by at least 1 eV in order to affect the Co valence and therefore to promote the charge transfer necessary for strong exchange coupling³³, a task hardly achievable.

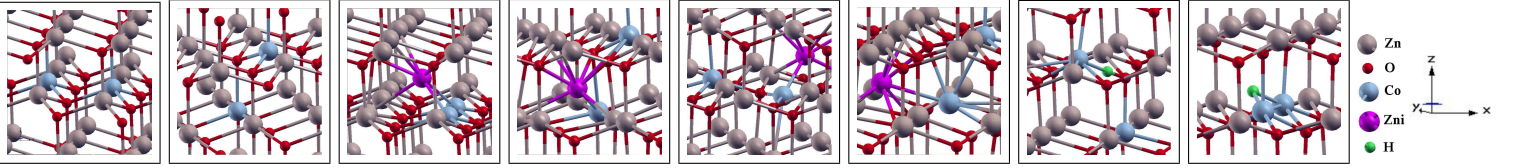
We test this conjecture by calculating the magnetic coupling between two Co^{2+} at various distances $d_{\text{Co-Co}}$. In table I we show the magnetic coupling energy E_M ($E_M > 0$ indicates ferromagnetic coupling), obtained as the total energy difference between the ferromagnetic (FM) and antiferromagnetic (AFM) configuration of a selection of supercells containing two Co^{2+} and one intrinsic defect far from both the Co^{2+} . Clearly the exchange interaction between two Co^{2+} is strong only at NN position, i.e. when the super-exchange interaction is effective. In this case the interaction is AFM in the a - b plane ($d_{\text{Co-Co}}=3.19\text{\AA}$) and FM along the c axis ($d_{\text{Co-Co}}=3.11\text{\AA}$). E_M however drops to zero already at second NN, regardless of the presence of additional intrinsic defects. In particular we show data for third NN (the data for second NN are similar) in presence of either Zn_i , H or V_O from which one has to conclude that RTF is not achievable by simply defect doping.

Figure 2 offers an insight on why Zn_i and V_O are unable to mediate RTF. We present the DOS of a 128 atom supercell containing one Co^{2+} and one intrinsic defect (V_O , Zn_i and H), and compare the case where the Co^{2+} and the defect are well separated in the cell with that in which they are at NN position. In the case of distant defects the DOS is essentially a superposition of that of Co^{2+} and the defect. Both Zn_i and H possess a filled hydrogenic level above the CBM and rather close to the Co d - t_2 minority levels. In contrast V_O displays a doubly occupied impurity level 1 eV above the VBT, almost at the same position of the minority Co- d e levels. Most importantly there is no evidence of interaction between Co^{2+} and the defect levels (the magnetic moment calculated from the Mulliken population is $\sim 2.6 \mu_B/\text{Co}$ for all three cases, similarly to the case of Co^{2+} only). This means that, despite the energy proximity of the defect levels to those of the Co 3d shell, the overlap of the hydrogenic wave-function at the Co site is only minimal. For this reason we conclude that the DIBE model as formulated cannot be sustained by the electronic structure of Co^{2+} in ZnO.

The right panels of Fig. 2 for NN defects give a different picture. In the case of both H and Zn_i there is a substantial charge transfer from the defects to the Co^{2+} resulting in a partial occupation of the minority t_2 levels and a reduction of the magnetic moment ($1.95 \mu_B/\text{Co}$ and $2.05 \mu_B/\text{Co}$ respectively for Zn_i and H). On-site repulsion moves upwards in energy all the Co 3d manifold and now the majority t_2 levels occupy the ZnO bandgap. In contrast, for V_O slight charge transfer from the Co 3d to the vacancy and hybridization move the 3d manifold downwards in energy and the doubly occupied V_O level spin-splits in the opposite direction to that of Co. Such a feature suggests that the exchange interaction be-

TABLE I: Calculated magnetic energy E_M for various magnetic centers and different dopants configuration. C1 and C2 are the two magnetic centers included in the simulation cell and their relative concentration (concentration of each center), D is the dopant with its concentration, d_{C1-C2} in the distance between the two center expressed both in Å and in NN shells. For some of the NN complexes we present the geometrical configuration (after relaxation in the pictures below).

C1 (x)	C2 (x)	D (y)	d_{C1-C2} (Å)	d_{C1-C2} (NN)	Position D	E_M (meV)	Fig.
Co (0.015)	Co (0.015)	–	3.19	1	–	-38	1
Co (0.015)	Co (0.015)	–	3.11	1	–	62	2
Co (0.015)	Co (0.015)	–	4.54	2	–	-1	-
Co (0.010)	Co (0.010)	Zn _i (0.010)	8.01	3	Far	-1	-
Co (0.010)	Co (0.010)	Zn _i ⁺ (0.010)	8.01	3	Far	1	-
Co (0.010)	Co (0.010)	H (0.010)	8.01	3	Far	0	-
Co (0.010)	Co (0.010)	V _O (0.010)	8.01	3	Far	-1	-
Co (0.015)	Co (0.015)	Zn _i (0.015)	3.180	1	Near	629	3
Co (0.015)	Co (0.015)	Zn _i (0.015)	2.551	1	Near	3	4
Co (0.015)	Co (0.015)	Zn _i (0.015)	2.914	1	Near	512	5
Co (0.015)	Co (0.015)	Zn _i (0.015)	2.557	1	Near	731	3
Co (0.015)	Co (0.015)	V _O (0.010)	2.585	1	Near	10	6
Co (0.015)	Co (0.015)	V _O (0.010)	2.795	1	Near	-103	-
Co (0.015)	Co (0.015)	V _O (0.010) & Zn _i	2.315	1	Near	899	-
Co (0.015)	Co (0.015)	H (0.010)	3.829	1	Near	12	7
Co (0.015)	Co (0.015)	H (0.010)	2.713	1	Near	296	8
CoV (0.015)	CoV (0.015)	–	5.55	2	–	-6	-
CoV (0.015)	CoV (0.015)	H (0.010)	2.30	1	Far	423	-
CoV (0.015)	CoV (0.015)	H (0.010)	2.27	1	Far	614	-
CoV (0.015)	CoV (0.015)	H (0.010)	5.55	2	Far	84	-
CoV (0.015)	CoV (0.015)	H (0.010)	4.51	2	Far	9	-
CoV (0.015)	CoV (0.015)	H (0.010)	6.94	3	Far	20	-



tween NN Co ions, when mediated by a defect, can be extremely large. This is indeed the case as demonstrated in table I where E_M for various Co-Co-defect complexes is presented. Such complexes effectively behave as small metallic clusters and it is of no surprise that the exchange energy increases quite dramatically for d_{Co-Co} around and below 2.5 Å, which is the NN distance in metallic Co.

Is this sufficient for RTF in the diluted phase? Unfortunately not. These interactions, although strong, are still short-range and therefore produce RTF only for x around the percolation limit. Moreover, the strong FM interactions require a ratio between Co and the relevant donor of 2:1, which at percolation means typical defect concentrations of around 10%. These are impossible to achieve for any of the defects investigated even under the most favorable conditions. Finally those complex structures, if abundant, should appear spectroscopically

with a substantial increase of the Co- d DOS in the ZnO bandgap.

Since Co²⁺ alone cannot be responsible for RTF at low dilution we have searched for other possible magnetic centers and found that Co²⁺-V_O pairs (CoV) overcome the limitations mentioned above. In figures 2d and 2e we present the DOS associated to the Co- d shell for both Co²⁺ and CoV, as compared with UPS from reference¹³. Clearly both Co²⁺ and CoV are compatible with UPS, in particular they both show a finite DOS at about -8 eV from E_F . This feature is absent in the DOS of both the Co-Zn_i and Co-H complexes, which instead present substantial contributions in the ZnO gap and therefore are incompatible with the spectroscopy. Moreover CoV is the only complex among the ones studied which maintains Co in the 2+ valence state.

CoV are also likely to be abundant. Our calculated V_O formation energy (see supplementary material) in zinc

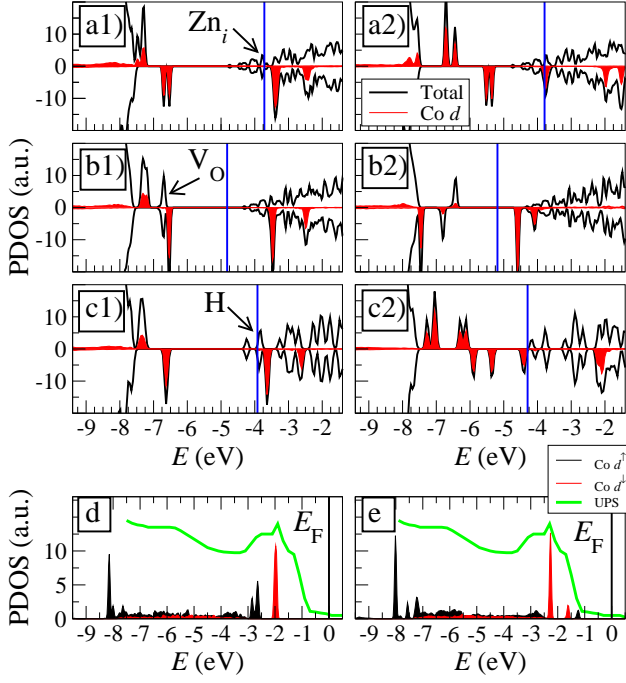


FIG. 2: Density of states for a ZnO 128 atom supercell with one Co^{2+} and one additional defect: a) Zn_i , b) V_O , and c) H. The left panels are for Co^{2+} and the defect well separated in the cell, while the right panels are for the NN position. The arrows indicate the relevant defect position. In d) and e) we present the Co 3 d density of states as compared with UPS data from reference¹³. d) Co^{2+} substitutional at the Zn site, e) Co^{2+} - V_O complex. The UPS signal has been aligned to the calculated DOS in order to have the first peak at the minority Co e states.

rich conditions is 0.65 eV, which suggests that the V_O concentration in ZnO can be as large as 1 % at equilibrium. Since Co does not introduce doping its presence will not change considerably the V_O formation energy. We have then only to establish whether the V_O sits preferentially close to a Co site. By using a 128 atom supercell we calculate a reduction in total energy of about 340 meV for Co and V_O moving from third to first NN (pairing energy). This is quite a large gain suggesting that most of the V_O are indeed likely to be close to Co ions. The large pairing energy also means that the relative concentration of CoV (x^{CoV}) with respect to that of Co^{2+} (x^{Co}) will increase upon oxygen absorbing processing. This is the case for both annealing in an oxygen poor atmospheres and long exposure to Zn and Ti vapours²⁶. In the first case one expects V_O migration to the Co sites, while in the second a preferential V_O formation close to Co. Finally we found that the pairing energy between two Co^{2+} is also large (~ 210 meV), while we do not find any substantial pairing interaction among the CoV in any charging configuration. We then expect an inhomogeneous distribution of the Co^{2+} , which in turn would lead to an inhomogeneous distribution of CoV and the formation of both high and low concentration regions.

Finally we have to establish whether CoV couple at long-range. Table I shows E_M for various CoV combinations. Similarly to the case of Co^{2+} also the magnetic coupling between two charge neutral CoV is remarkably weak already at second NN (-6 meV). However, when an additional electron donor is present, the situation changes dramatically with second and third NN magnetic coupling reaching up respectively to $E_\text{M} \sim 80$ meV and $E_\text{M} \sim 20$ meV. Note that we cannot exclude an even longer interaction range, which however is hardly accessible in our simulations since the size of the supercells becomes prohibitively large.

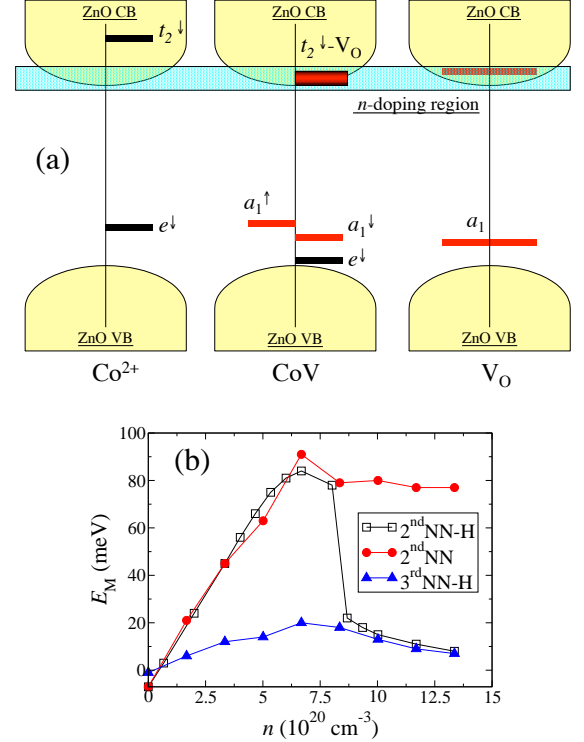


FIG. 3: CoV impurity band. (a) level diagram for Co^{2+} , V_O and CoV, (b) E_M for two 2nd NN CoV as a function of the donor impurity band electron density. The electron density $6.7 \cdot 10^{20} \text{ cm}^{-3}$ corresponds to one electron every two CoV.

Why does CoV sustain long range coupling while Co^{2+} does not? The cartoon of Fig. 3a shows the electronic structure of Co^{2+} , V_O and CoV. The main feature is that the Co^{2+} empty t_2 minority state broadens in CoV and forms a t_2 - V_O hybrid level right at the CBM. This extends in space over the the first shell of Zn ions and an impurity band forms already at tiny concentrations. Such a band can be easily n -doped. Thus, while for Co^{2+} the only exchange mechanisms available either involve virtual transitions or weak s - d ³⁸ exchange interaction with hydrogenic orbitals, for CoV strong carrier-mediated magnetic interaction is possible. In figure 3b we show E_M for two CoV in a 128 atom unit cell as a function of the electron doping. This is introduced by either moving E_F in our simulations or by explicitly introducing an H ion

in the supercell. Clearly E_M depends strongly on the occupation of the impurity band, with a maximum at half filling ($n=6.7 \times 10^{20} \text{ cm}^{-3}$) and vanishing for $n=0$ (empty band).

Thus DFT offers us a mechanism for the ferromagnetism in (Zn,Co)O based on two magnetic centers. Co^{2+} is responsible only for short range coupling, while CoV can instead sustain long range interaction via a fractionally filled impurity band. Can this alone produce RTF? Percolation theory³⁹ sets a strict condition for a magnetic ground state of diluted systems: the concentration of magnetic impurity should exceed the percolation threshold x_c . This depends on the range of the interaction and for the fcc lattice we find 19.8%, 13.7% and 6.2% for interaction extending respectively to 1st, 2nd and 3rd NN⁴⁰. Therefore our two-center model already produces long range ferromagnetism at $x^{\text{CoV}} > x_c \sim 6\%$. However, we do not need such a large x for observing hysteresis in the M - H curve at room temperature (i.e. for explaining the various experimental claims). This can be achieved below x_c since one just needs a number of percolating clusters large enough to be superparamagnetically blocked. Note that “clusters” here mean regions where x is locally larger than x_c . The presence of CoV pushes this limit far below the 20% needed by Co^{2+} and by the recently proposed model where the magnetism originates from uncompensated spins at the surface of antiferromagnetic clusters⁴¹.

The size of those clusters can be estimated by considering coherent rotation of the magnetization over an anisotropy barrier $DN_B S^2$ (D is the zero-field splitting, N_B the number of magnetic ions magnetically blocked and S the Co spin). By taking $D = 2.76 \text{ cm}^{-1}$ from EPR measurements¹⁷ we obtain the estimate $N_B \sim 800$ for a blocking temperature $T_B = 300 \text{ K}$. This however is rather conservative. In granular magnets random dipolar interaction⁴², random magnetic anisotropy⁴³ or spinodal decomposition⁴⁴ can push T_B to values considerably larger than those predicted for single particle coherent rotation (up to a factor 5). Thus we estimate N_B in the range of 250 magnetic ions. Therefore, an observation of a hysteresis requires the existence of regions where 250 CoV ions interacting at 3rd NN exist at concentrations larger than $\sim 6\%$. Indeed this is a rather modest requirement.

In Fig. 4a we present typical cluster distributions $P(N)$ as a function of the cluster size N for various concentrations of Co^{2+} and CoV. These have been obtained by filling randomly a wurtzite lattice comprising 10^6 sites. As expected $P(N)$ moves from small to large clusters as x^{CoV} is increased with respect to x^{Co} . In particular one notes that already for $x^{\text{CoV}} = 2\%$ large clusters appear in the distribution, which becomes bi-modal at $x^{\text{CoV}} > 6\%$, i.e. above x_c . We emphasize that these $P(N)$ have been obtained from a completely random distribution, i.e. neglecting the tendency to clustering suggested by the pairing energy.

Finally we investigate the thermodynamical properties of our two center model by performing Monte Carlo sim-

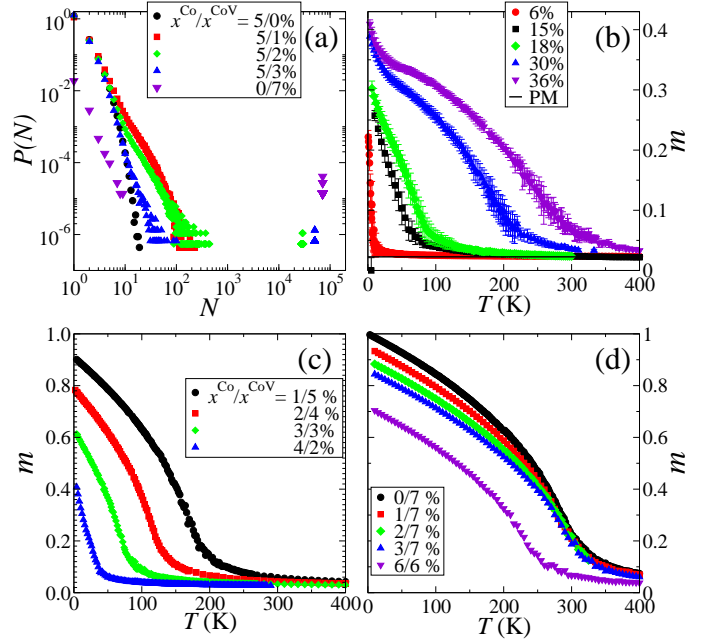


FIG. 4: Monte Carlo simulations for the two center model: (a) cluster distribution $P(N)$ as a function of the number N of magnetic ions in the cluster for different x^{Co} and x^{CoV} ($x^{\text{Co}}/x^{\text{CoV}}$); (b) magnetization curves $m(T)$ at different Co concentration for $x^{\text{Co}}/x^{\text{CoV}} = 5$; (c) $m(T)$ for a total Co concentration of 6% and different $x^{\text{Co}}/x^{\text{CoV}}$; (d) $m(T)$ for x^{CoV} above percolation (7%) and various x^{Co} ($x^{\text{Co}}/x^{\text{CoV}}$).

ulations for a Heisenberg energy ($|\mathbf{S}_i| = 1$)

$$\mathcal{H}_{\text{eff}} = \sum_{\langle i,j \rangle}^{\text{Co, CoV}} J_{ij} \mathbf{S}_i \cdot \mathbf{S}_j + \sum_i^{\text{Co, CoV}} D(\mathbf{S}_i \cdot \hat{n})^2. \quad (1)$$

The exchange parameters are chosen to mimic the short and long range exchange between Co^{2+} and CoV respectively. At NN J_{ij} is AFM for Co^{2+} pairs (15 meV) and FM for CoV pairs (50 meV) and between Co^{2+} and CoV (50 meV). Moreover it extends to 2nd (15 meV) and 3rd NN (5 meV) for CoV pairs. The last term accounts for an hard-axis easy-plane anisotropy ($|\hat{n}| = 1$)¹⁷. Note that we implicitly assume doping in the CoV impurity band and neglect the NN FM component of the exchange between Co^{2+} pairs. Given the uncertainty over the precise microscopic configuration and the relative abundance of the various complexes (Table I) our numerical values are only representative and certainly conservative. However, even with this choice $T_C = 250 \text{ K}$ above percolation ($x^{\text{CoV}} = 7\%$) suggesting that RTF is indeed possible.

In Fig. 4b we present the reduced magnetization $m = M/M_s$ as a function of T for different Co concentrations, while keeping $x^{\text{Co}}/x^{\text{CoV}} = 5$. The magnetization curves show a transition from a concave upwards shape at low concentrations to a convex one for high. As the concentration increases one encounters the two percolation thresholds, respectively for CoV and for Co. This produces the change in shape, which however is complete

only above 20%, i.e. when the Co^{2+} 's start to percolate. Interestingly m never reaches 1 because of the strong NN AFM interaction among Co.

We also investigate the interplay between Co^{2+} and CoV. In figure Fig. 4c $m(T)$ is calculated by keeping the total Co concentration to 6% and by varying the ratio between x^{Co} and x^{CoV} , while in Fig. 4d we keep $x^{\text{CoV}} = 7\%$ (above percolation) and change x^{Co} . In both pictures x^{Co} is well below the percolation threshold for NN and the high-temperature region of $m(T)$ is almost entirely dominated by x^{CoV} . For instance one may note that for $x^{\text{CoV}} = 5\%$ $m(T)$ approaches zero roughly at the same T regardless of whether x^{Co} is 1% (Fig. 4c) or 25% (Fig. 4b for a total concentration of 30%). In contrast the amount of Co^{2+} affects the low temperature region, where the strong AFM interaction can drastically alter the total magnetic moment. For instance $m(0)$ drops from 1 to about 0.8 if x^{Co} is increased from 1 to 3%, by keeping $x^{\text{CoV}} = 7\%$.

We are now in a position to propose a phase diagram for (Zn,Co)O based on the relative concentration of Co^{2+} and CoV (Fig. 5). The most important feature is the presence of what we called a blocked superparamagnetic phase. This is below x_c^{CoV} and x_c^{Co} , but nevertheless al-

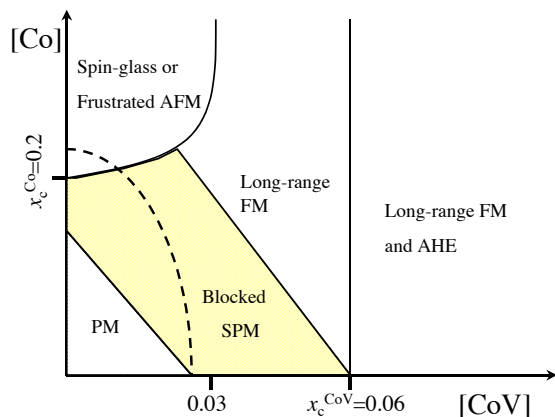


FIG. 5: Proposed phase diagram for (Zn,Co)O as a function of the relative concentrations of Co and CoV. The yellow area is the blocked superparamagnetic (SPM) region, where both magnetic moment and hysteresis can be detected. The dashed line at small x delimits the region where most of the experiments are conducted. Finally the FM region is partitioned into two regions depending on whether or not anomalous Hall effect can be detected.

lows one the detection of both a net magnetic moment and hysteresis at room-temperature. For larger x a long-range FM ground state emerges, which however is limited by the short range AFM interaction of the Co ions. Therefore we predict either a frustrated antiferromagnet or a spin-glass for $x^{\text{Co}} > x_c^{\text{Co}}$ and $x^{\text{CoV}} \ll x^{\text{Co}}$. We emphasize that bulk measurements (hysteresis or magnetization) can hardly distinguish between the FM and the blocked superparamagnetic phase, and more local

probes are needed. In particular further insights would be provided by a thorough analysis of small angle neutron scattering data similar to the case of disordered ferromagnets⁴³. Alternatives may be muon rotation, high resolution EPR and energy-dispersive X-ray spectroscopy.

Finally we partition the long-range FM region into two regions separated by the CoV percolation threshold x_c^{CoV} . For $x^{\text{CoV}} > x_c^{\text{CoV}}$ percolation among CoV is achieved and one expects measurable conductivity from the impurity band. Since the exchange is strong an anomalous Hall effect (AHE) should be detected. This is not expected for ferromagnetism below x_c^{CoV} since the conductivity is then dominated by band conductivity which is weakly affected by Co^{2+} , given the small exchange. Note that this phase diagram says little about the overall conductivity of (Zn,Co)O, which in turn can be determined by electrons in the conduction band. Moreover, the precise location of the phase boundaries depends on details such as the concentration of electron donors. In the extreme case of fully compensated samples the blocked superparamagnetic phase may even disappear entirely.

In conclusion, by using a combination of DFT and Monte Carlo simulations, we have demonstrated that the observed RTF in (Zn,Co)O can be attributed to blocked superparamagnetism. This develops at concentrations below those required by long-range ferromagnetism. However, even this model requires a second magnetic dopant in addition to Co^{2+} substituting Zn, capable of mediating magnetic interaction beyond nearest neighbours. We have identified the Co- V_O pair as the most likely candidate and demonstrated that such center can indeed promote long range coupling, if additional n doping is present. These findings draw a new roadmap for designing diluted magnetic oxides, where the engineering of intrinsic defects play the leading role. For instance paramagnetic samples can be turned ferromagnetic by prolonged exposure to Ti vapours, which produce high concentrations of V_O ²⁶.

Methods

Density functional theory calculations have been performed by using our newly developed approximate version of the self-interaction correction scheme (ASIC)³⁵. This is implemented numerically in the localized basis set code *Siesta*⁴⁵. Here the ASIC scaling parameter α was set to 1/2, which is the value appropriate for describing the electronic structure of mid- to wide-gap semiconductors³⁵. In all the simulations we have considered unit cells ranging from 128 to 256 atoms. The basis set used was as follows: Zn: DZ-*s*, DZ-*p*, SZ-*d*, O: DZ-*s*, DZ-*p*, SZ-*d*, Co: DZ-*s*, DZP-*p*, DZ-*d* (SZ=single zeta, DZ=double zeta, DZP=double zeta polarized⁴⁵). The grid cutoff (equivalent to plane wave-cutoff) was 650 Ry and we have considered 18 k -points in the full Brillouin

zone for the 128 atom cell and appropriate scaling for other cells. Standard conjugate gradient geometrical relaxation was performed until the forces were smaller than 0.04 eV/Å.

Monte Carlo simulations were performed with the Metropolis algorithm as implemented in a home-made package. Typical simulation cells for the two center Heisenberg model contain between 1,600 to 5,000 mag-

netic ions and we always use periodic boundary conditions. The systems are equilibrated until an initially AFM and FM replica have converged to the same value (typically 10,000 steps) and then the Monte Carlo measurements are taken by sampling 60,000 new steps. Disorder averages are taken over 32 different samples at each concentration. T_C for the case of $x^{\text{CoV}} = 7\%$ is evaluated from the specific heat (see supplementary materials).

- ¹ V.E. Wood and A.E. Austin, Magnetoelectric interaction phenomena in crystals [London: Gordon and Breach (1975)].
- ² Special issue on Transparent Conducting Oxides, edited by D.S. Ginley and C. Bright [MRS Bull. **25** (2000)]
- ³ D.D. Awschalom, D. Loss and N. Samarth, Semiconductor Spintronics and Quantum Computing, [Springer, Heidelberg, 2002]
- ⁴ M.H. Huang, S. Mao, H. Feick, H. Yan, Y. Wu, H. Kind, E. Weber, R. Russo and P. Yang, Room-Temperature Ultraviolet Nanowire Nanolasers, *Science* **292**, 1897-1899 (2001).
- ⁵ M. Kroutvar, Y. Ducommun, D. Heiss, M. Bichler, D. Schuh, G. Abstreiter and J.J. Finley, Optically programmable electron spin memory using semiconductor quantum dots, *Nature (London)* **432**, 81-84 (2004).
- ⁶ A.H. MacDonald, P. Schiffer and N. Samarth, Ferromagnetic semiconductors: moving beyond (Ga,Mn)As, *Nature Materials* **4**, 195-202 (2005).
- ⁷ K. Ueda, H. Tabata and T. Kawai, Magnetic and electric properties of transition-metal-doped ZnO films, *Appl. Phys. Lett.* **79**, 988-990 (2001).
- ⁸ K. Rode, A. Anane, R. Mattana, J.-P. Contour, O. Durand and R. LeBourgeois, Magnetic semiconductors based on cobalt substituted ZnO, *J. Appl. Phys.* **93**, 7676-7678 (2003).
- ⁹ W. Prellier, A. Fouchet, B. Mercey, Ch. Simon and B. Raveau, Laser ablation of Co:ZnO films deposited from Zn and Co metal targets on (0001) Al₂O₃ substrates, *Appl. Phys. Lett.* **82**, 3490-3492 (2003).
- ¹⁰ M. Venkatesan, C.B. Fitzgerald, J.G. Lunney and J.M.D. Coey, Anisotropic Ferromagnetism in Substituted Zinc Oxide, *Phys. Rev. Lett.* **93**, 177206 (2004).
- ¹¹ H.-J. Lee, S.-Y. Jeong, C.R. Cho and C.H. Park, Study of diluted magnetic semiconductor: Co-doped ZnO, *Appl. Phys. Lett.* **81**, 4020-4022 (2002).
- ¹² A.C. Tuan et al., Epitaxial growth and properties of cobalt-doped ZnO on α -Al₂O₃ single-crystal substrates, *Phys. Rev. B* **70**, 054424 (2004).
- ¹³ M. Kobayashi et al., Characterization of magnetic components in the diluted magnetic semiconductor Zn_{1-x}Co_xO by x-ray magnetic circular dichroism, *Phys. Rev. B* **72**, 201201(R) (2005).
- ¹⁴ S.C. Wi et al., Electronic structure of Zn_{1-x}Co_xO using photoemission and x-ray absorption spectroscopy, *Appl. Phys. Lett.* **84**, 4233-4235 (2004).
- ¹⁵ Y.Z. Peng, T. Liew, T.C. Chong, W.D. Song, H.L. Li and W. Liu, Growth and characterization of dual-beam pulsed-laser-deposited Zn_{1-x}Co_xO thin films, *J. Appl. Phys.* **98**, 114909 (2005).
- ¹⁶ A.S. Risbud, N.A. Spaldin, Z.Q. Chen, S. Stemmer and R. Seshadri, Magnetism in polycrystalline cobalt-substituted zinc oxide, *Phys. Rev. B* **68**, 205202 (2003).
- ¹⁷ Sati et al., Magnetic Anisotropy of Co²⁺ as Signature of Intrinsic Ferromagnetism in ZnO:Co, *Phys. Rev. Lett.* **96**, 017203 (2006).
- ¹⁸ G.L. Liu et al., High T_C ferromagnetism of Zn_{1-x}Co_xO diluted magnetic semiconductors grown by oxygen plasma-assisted molecular beam epitaxy, *Appl. Phys. Lett.* **90**, 052504 (2007).
- ¹⁹ L.S. Dorneles et al., Magnetic and structural properties of Co-doped ZnO thin films, *J. Magn. Magn. Mater.* **310**, 2087-2088 (2007).
- ²⁰ A. Dinia, G. Schmerber, C. Mény, V. Pierron-Bohnes and E. Beaurepaire, Room-temperature ferromagnetism in Zn_{1-x}Co_xO magnetic semiconductors prepared by sputtering, *J. Appl. Phys.* **97**, 123908 (2005).
- ²¹ J. Cui and U. Gibson, Thermal modification of magnetism in cobalt-doped ZnO nanowires grown at low temperatures, *Phys. Rev. B* **74**, 045416 (2006).
- ²² H.S. Hsu et al., Evidence of oxygen vacancy enhanced room-temperature ferromagnetism in Co-doped ZnO, *Appl. Phys. Lett.* **88**, 242507 (2006).
- ²³ X. Han, G. Wang, J. Jie, X. Zhu and J.G. Hou, Properties of Zn_{1-x}Co_xO thin films grown on silicon substrates prepared by pulsed laser deposition, *Thin. Sol. Films* **491**, 249-252 (2005).
- ²⁴ N. Khare, M.J. Kappers, M. Wei, M.G. Blamire and J.L. MacManus-Driscoll, Defect-induced ferromagnetism in Co-doped ZnO, *Adv. Mat.* **18**, 1449-1452 (2006).
- ²⁵ H.-J. Lee et al., Hydrogen-induced ferromagnetism in Zn-CoO, *Appl. Phys. Lett.* **88**, 062504 (2006).
- ²⁶ F.A. Selim, M.H. Weber, D. Solodovnikov and K.G. Lynn, Nature of native defects in ZnO, *Phys. Rev. Lett.* **99**, 085502 (2007).
- ²⁷ S. Lany and A. Zunger, Dopability, intrinsic conductivity and nonstoichiometry of transparent conducting oxides, *Phys. Rev. Lett.* **98**, 045501 (2007).
- ²⁸ A. Janotti and C.G. van de Walle, Hydrogen multicentre bonds, *Nature Materials* **6**, 44 (2007).
- ²⁹ D.A. Schwartz and D.R. Gamelin, Reversible 300 K ferromagnetic order in a diluted magnetic semiconductor, *Adv. Mat.* **16**, 2115-2119 (2004).
- ³⁰ A. O. Ankiewicz, Electron paramagnetic resonance in transition metal-doped ZnO nanowires, *J. Appl. Phys.* **101**, 024324 (2007).
- ³¹ T. Dietl, H. Ohno, F. Matsukura, J. Cibert and D. Ferrand, Zener model description of ferromagnetism in zinc-blende magnetic semiconductors, *Science* **287**, 1019 (2000).
- ³² J.B. Goodenough, *Magnetism and chemical bond* [Wiley-Interscience, New York-London, 1963].
- ³³ J.M.D. Coey, M. Venkatesan and C.B. Fitzgerald, Donor

- impurity band exchange in dilute ferromagnetic oxides, *Nature Materials* **4**, 173 (2005).
- ³⁴ M. Wierzbowska, D. Sánchez-Portal and S. Sanvito, Different origin of the ferromagnetic order in (Ga,Mn)As and (Ga,Mn)N, *Phys. Rev. B* **70**, 235209, (2004).
 - ³⁵ C. Das Pemmaraju, T. Archer, D. Sánchez-Portal and S. Sanvito, Atomic-orbital-based approximate self-interaction correction scheme for molecules and solids, *Phys. Rev. B* **75**, 045101, (2007).
 - ³⁶ A. Akande and S. Sanvito, Exchange parameters from approximate self-interaction correction scheme, *J. Chem. Phys.* **127**, 034112, (2007).
 - ³⁷ M. Toyoda, H. Akai, K. Sato and H. Katayama-Yoshida, Electronic structures of (Zn, TM)O (TM: V, Cr, Mn, Fe, Co, and Ni) in the self-interaction-corrected calculations, *Physica B* **376-377**, 647 (2006).
 - ³⁸ B.E. Larson, K.C. Hass, H. Ehrenreich and A.E. Carlsson, Theory of exchange interactions and chemical trends in diluted magnetic semiconductors, *Phys. Rev. B* **37**, 4137 (1988).
 - ³⁹ D. Stauffer and A. Aharony, Introduction to percolation theory, [Taylor & Francis, London 1994].
 - ⁴⁰ J. Osorio-Guillén, S. Lany, S.V. Barbash and A. Zunger, Nonstoichiometry as a source of magnetism in otherwise nonmagnetic oxides: magnetically interacting cation vacancies and their percolation, *Phys. Rev. B* **75**, 184421 (2007).
 - ⁴¹ T. Dietl, T. Andrearczyk, A. Lipińska, M. Kiećana, M. Tay and Y. Wu, Origin of ferromagnetism in $\text{Zn}_{1-x}\text{Co}_x\text{O}$ from magnetization and spin-dependent magnetoresistance measurements, *Phys. Rev. B* **76**, 155312 (2007).
 - ⁴² P. Allia, M. Coisson, P. Tiberto, F. Vinai, M. Knobel, M.A. Novak and W.C. Nunes, Granular Cu-Co alloys as interacting superparamagnets, *Phys. Rev. B* **64**, 144420 (2001).
 - ⁴³ J. Löffler, H.-B. Braun and W. Wagner, Magnetic correlations in nanostructured ferromagnets, *Phys. Rev. Lett.* **85**, 1990 (2000).
 - ⁴⁴ K. Sato, T. Fukushima and H. Katayama-Yoshida, Super-Paramagnetic Blocking Phenomena and Room-Temperature Ferromagnetism in Wide Band-Gap Dilute Magnetic Semiconductor (Ga, Mn)N, *Jpn. J. Appl. Phys.* **46**, L682 (2007).
 - ⁴⁵ J.M. Soler, E. Artacho, J.D. Gale, A. Garcia, J. Junquera, P. Ordejón and D. Sanchez-Portal, The SIESTA method for ab initio order-N materials simulation, *J. Phys.: Condens. Matter* **14**, 2745 (2002).

Acknowledgment

This work is sponsored by Science Foundation of Ireland under the grants SFI02/IN1/I175 and 05/IN1/I853. We thank TCHPC and ICHEC for providing computational support.